



HAL
open science

The effects of explosive-driven shocks on the natural remanent magnetization and the magnetic properties of rocks

J. Gattacceca, A. Lamali, P. Rochette, M. Boustie, L. Berthe

► **To cite this version:**

J. Gattacceca, A. Lamali, P. Rochette, M. Boustie, L. Berthe. The effects of explosive-driven shocks on the natural remanent magnetization and the magnetic properties of rocks. *Physics of the Earth and Planetary Interiors*, 2007, 162 (1-2), pp.85-98. 10.1016/j.pepi.2007.03.006 . hal-00532102

HAL Id: hal-00532102

<https://hal.science/hal-00532102v1>

Submitted on 4 Nov 2010

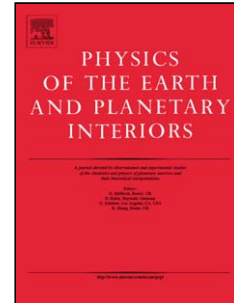
HAL is a multi-disciplinary open access archive for the deposit and dissemination of scientific research documents, whether they are published or not. The documents may come from teaching and research institutions in France or abroad, or from public or private research centers.

L'archive ouverte pluridisciplinaire **HAL**, est destinée au dépôt et à la diffusion de documents scientifiques de niveau recherche, publiés ou non, émanant des établissements d'enseignement et de recherche français ou étrangers, des laboratoires publics ou privés.

Accepted Manuscript

Title: The effects of explosive-driven shocks on the natural remanent magnetization and the magnetic properties of rocks

Authors: J. Gattacceca, A. Lamali, P. Rochette, M. Boustie, L. Berthe



PII: S0031-9201(07)00058-1
DOI: doi:10.1016/j.pepi.2007.03.006
Reference: PEPI 4803

To appear in: *Physics of the Earth and Planetary Interiors*

Received date: 20-10-2006
Revised date: 16-3-2007
Accepted date: 21-3-2007

Please cite this article as: Gattacceca, J., Lamali, A., Rochette, P., Boustie, M., Berthe, L., The effects of explosive-driven shocks on the natural remanent magnetization and the magnetic properties of rocks, *Physics of the Earth and Planetary Interiors* (2007), doi:10.1016/j.pepi.2007.03.006

This is a PDF file of an unedited manuscript that has been accepted for publication. As a service to our customers we are providing this early version of the manuscript. The manuscript will undergo copyediting, typesetting, and review of the resulting proof before it is published in its final form. Please note that during the production process errors may be discovered which could affect the content, and all legal disclaimers that apply to the journal pertain.

The effects of explosive-driven shocks on the natural remanent magnetization and the magnetic properties of rocks

J. Gattacceca^{1*}, A. Lamali², P. Rochette¹, M. Boustie³, L. Berthe⁴

¹CEREGE (CNRS/Université Paul Cézanne), BP 80, 13545 Aix-en-Provence Cedex 4, France

²CRAAG, BP 63 Bouzaréah, 16340 Alger, Algeria

³LCD (CNRS/ENSMA), BP 40109, 8696 Futuroscope Cedex, France

⁴LALP (CNRS), 94114 Arcueil cedex, France

* corresponding author

Accepted Manuscript

1 **1. Introduction**

2 The effects of shock waves on the natural remanent magnetization (NRM) and the intrinsic
3 magnetic properties of geological materials remain poorly known. Still, hypervelocity impact
4 phenomena are of primary importance in the evolution of many extraterrestrial bodies and of
5 Earth. Hence the magnetic anomalies associated with impact basins on Mars (Hood et al.,
6 2003), the Moon (Halekas et al., 2003) or on Earth (Pilkington and Grieve, 1992) cannot be
7 interpreted with certainty. Also, shock-induced changes of rock magnetic properties should be
8 taken into account when studying the magnetic signature of terrestrial impact structures.

9 Since the 1970's, efforts have been devoted to the experimental study of remagnetization of
10 rocks upon impact, whereas little has been done about the shock-induced modifications of
11 their intrinsic magnetic properties. Different techniques have been used to generate shock
12 waves in a variety of geological materials: air guns accelerating aluminum or copper
13 projectiles (Hornemann et al., 1975; Pohl et al., 1975; Martelli and Newton, 1977; Cisowski
14 and Fuller, 1978; Srnka et al., 1979; Dickinson and Wasilewski, 2000), explosives (Hargraves
15 and Perkins, 1969; Pesonen et al., 1997), free falling mass (Kletetschka et al., 2004).
16 Common limitations are the difficulty in calibrating the pressure in the shocked sample and
17 the recovery of intact samples due to brecciation of the target. On the other hand modern
18 mechanical impact experiments using gas guns can recover intact samples with good pressure
19 calibration (e.g. Louzada et al., in press). Recently, the use of laser shocks allowed a good
20 estimate of the demagnetization of saturation isothermal remanent magnetization up to 5 GPa
21 (Gattacceca et al., 2006), but the pressure gradient was limited to a few millimeters inside the
22 sample, making it impossible to study the changes in intrinsic magnetic properties. Despite
23 these numerous experiments, the effects of shock waves on magnetization and magnetic
24 properties are not clearly understood in particular because of the numerous parameters that
25 may have an influence: shock intensity and duration, ambient field, magnetic mineralogy,
26 rheology, magnetization existing prior to shock, and temperature.

27 In this paper, we present new experiments in which different geological materials were
28 impacted using a high-order explosive (penthrite). The shock wave was modelled numerically
29 and we studied the effects of shock on the NRM and on the intrinsic magnetic properties of
30 the rocks.

31 **32 2. Material and methods**

33 Four different lithologies were studied: a Quaternary alkaline basalt (from the Bas-Vivarais
34 area, France, described in Rochette et al. (1993), a Tertiary quartzitic microdiorite

35 ("esterellite", from the Estérel range near the southeastern coast of France), a Permian
36 rhyolitic pyroclastic rock from the same area (Vlag et al., 1997), and a Precambrian-
37 Ordovician pyrrhotite-rich metamorphic schist from Wilson Terrane (Northern Victoria Land,
38 Antarctica). This choice was guided by the differences in magnetic mineralogy and magnetic
39 properties among these four lithologies.

40 The shock wave was driven into the samples using a high-order explosive (penthrite, PETN).
41 The shocked samples were large blocks in the range 10-20 kg. A flat surface was cut using a
42 circular saw. The sample was then placed in a large (0.3 m³) plastic container half-filled with
43 gravel. A penthrite detonator (0.2 g of penthrite contained in an aluminium cylinder of
44 external diameter 7.3 mm and thickness 0.5 mm) was fixed in direct contact with the flat,
45 locally polished surface of the sample. The container was then filled with gravel. The
46 penthrite was detonated remotely using a non-electric detonating wire. The outdoor
47 experimental setting contained no metallic parts except the aluminium cylinder containing the
48 penthrite, and no electromagnetic signal is expected during the detonation. Therefore we did
49 not use any system of magnetic field control and assume that the magnetic field seen by the
50 sample is the local geomagnetic field ($I = 59^\circ$, 46 μT). Each sample was oriented so that its
51 original NRM made an angle of about 90° with the local field. After recovery of the shocked
52 samples, we drilled an oriented core (\varnothing 2.5 cm) perpendicular to the flat surface and centred
53 on the impact. This core was in turn cut in 10 oriented $4 \times 4 \times 3 \text{ mm}^3$ parallelepipeds with a
54 wire saw (Fig. 1). Note that the upper few millimetres have been lost during the explosion for
55 the basalt (3 mm) and the rhyolite (8 mm). In the following, the sample numbers correspond
56 to the depth (in mm) of the centre of the 3 mm-high parallelepipeds from the original surface.
57 All magnetic analyses were performed at CEREGE (Aix-en-Provence, France). The
58 magnetization measurements were performed with a 2G Enterprises DC SQUID
59 magnetometer and data processed with Paleomac software (Cogné, 2003). Magnetic
60 susceptibility measurements and thermomagnetic analyses were performed with an Agico
61 KLY2-CS2 apparatus. Hysteresis loops were studied with a Princeton Micromag VSM
62 apparatus.

63

64 **3. Shock modelling**

65 In order to estimate the stress field induced in the samples by the explosions, a numerical
66 simulation of the experiments was performed. For this purpose, the Radioss code
67 [www.mecalog-group.fr] has been used in a 2D axisymmetric configuration. The explosive
68 PETN has been modelled by a Johnson Wilkins Lee law (Wilkins, 1999):

$$69 \quad P = A \left(1 - \frac{\omega}{R_1 V} \right) \exp(-R_1 V) + B \left(1 - \frac{\omega}{R_2 V} \right) \exp(-R_2 V) + \frac{\omega E}{V}$$

70 where P is the pressure, A , B , R_1 and R_2 are empirical parameters, ω is the Grüneisen
71 coefficient, E is the internal energy and V is the relative volume.

72 The modelled target material is a basalt described by an elasto-plastic constitutive law
73 coupled to the Mie-Grüneisen equation of state with reference to the Hugoniot through a
74 linear relationship between shock speed D and particle velocity u : $D = C_0 + s \cdot u$, where C_0 is
75 the sound speed and s is an empirical parameter. All the parameters used in the simulation are
76 listed in table 1. In the model, the diameter of the basalt has been taken large enough (6 cm)
77 to avoid lateral reverberations on the free surface during the duration of observation of the
78 phenomena (first pass of the shock).

79 The modelled evolution of stress versus time at various depths is given in Fig. 2. The shock
80 applied by the explosion has an almost triangular shape, with a peak pressure of 30 GPa and a
81 duration of about 1 μ s. The peak pressure decays to 5 GPa at only 20 mm. At depths greater
82 than 5 mm, following the compression the material is submitted to a tensile stress, due to the
83 lateral release initiated at the rim of the explosive charge, which generates expansion when
84 crossing behind the main shock.

85 According to the assumptions made for this simulation (homogeneous, isotropic and non
86 porous rock), and the variability of the intrinsic petrophysical parameters among the four
87 different samples (for instance bulk density is 2270 kg.m⁻³ for the rhyolite, 2700 kg.m⁻³ for
88 the microdiorite and the schist, and 3000 kg.m⁻³ for the basalt), we provide here only an
89 estimate of the stress field into the samples. Based on this estimate, the depth scale for each
90 shocked sample can be converted to a peak pressure scale (Fig. 3).

91

92 **4. Thermal modelling**

93 Because of the generation of the shock by a high explosive, an important heat flux is
94 transferred to the target. The temperature profile applied to the target by this explosion has
95 been calculated using the thermomechanical code Carte (Auroux and Deleignies, 2003) from
96 the Commissariat à l'Energie Atomique (CEA, France). A maximum temperature of about
97 4500°C is applied during about 1 μ s. A simulation of the dissipation of this heat into the
98 target has been performed using a heat conduction simulation with FEMLAB 3.1 code (from
99 COMSOL company). Physical properties introduced in the code are given in Table 1. The
100 temperature profile with depth is given in figure 4 and shows that the zone affected by a
101 significant heating (temperature > 50 °C) is restricted to the first upper micrometers. As a

102 consequence, no thermal effect is expected at all on the magnetization and the magnetic
103 properties of the studied samples.

104 On the other hand, the shock wave itself is accompanied by a transient increase of
105 temperature. For pressure below the elastic limit of the rock (~ 5 GPa for a basalt), this
106 increase is negligible ($\sim 10^\circ\text{C}$). For pressure greater than the elastic limit, the increase in
107 temperature can be estimated to about 50°C at 10 GPa and 100°C at 20 GPa (e.g. Stöffler et
108 al., 1991 and references therein).

109

110 **5. Pre-shock magnetization and magnetic properties of the studied materials**

111 Thermomagnetic curves (Fig. 5) allow the determination of the main magnetic carrier in
112 the samples. The basalt has a main Curie temperature (T_c) of 50°C indicating Ti-rich
113 titanomagnetite of composition $\text{Fe}_{0.25}\text{Ti}_{0.75}\text{O}_4$ (Dunlop and Özdemir, 1997). A second, less
114 substituted titanomagnetite population is evidenced by the blocking temperature spectrum of
115 thermoremanence that extends up to 350°C interval (Fig. 5). The microdiorite has $T_c = 575^\circ\text{C}$
116 indicating almost pure magnetite. This is confirmed by the observation of a Verwey transition
117 at 114°K . The rhyolite has $T_c = 650^\circ\text{C}$ indicating titanohematite. The thermomagnetic curve
118 for the schist shows the γ transition (antiferromagnetic to ferrimagnetic) of hexagonal
119 pyrrhotite at 220°C , $T_c = 280^\circ\text{C}$ of hexagonal pyrrhotite and $T_c = 320^\circ\text{C}$ of monoclinic
120 pyrrhotite. Hysteresis loops are in agreement with these interpretations (Fig. 6). For the
121 rhyolite, the wasp-waisted hysteresis loop evidences the existence of a minor amount of spinel
122 (titanomagnetite or titanomaghemite) in addition to titanohematite.

123 In view of the pressure profile in the samples (§3) and the temperature increase associated
124 to the shock wave (§4), no thermal effect is expected on the remanent magnetization or the
125 magnetic mineralogy of the studied rocks. Only for the basalt that has the lowest blocking
126 temperatures, a partial TRM acquisition (about 5-10% of the total TRM, see Fig. 5) is
127 possible up to a distance of 10 mm away from the point of explosion, the temperature increase
128 at this distance being $\sim 50^\circ\text{C}$.

129 To study the natural variability of magnetic properties within the studied rocks, we drilled
130 a $\varnothing 2.5$ cm core parallel to the direction of the impact and more than 10 cm away from the
131 impact point. This core was cut in smaller samples whose hysteresis properties (B_c :
132 coercivity, B_{cr} : coercivity of remanence, M_s : saturation magnetization, M_{rs} : remanent
133 magnetization at saturation), magnetic susceptibility, anisotropy of magnetic susceptibility
134 (AMS) and NRM were measured. The results show no significant variation of the NRM
135 intensity and magnetic properties with depth or mass of the sample. The only exception is a

136 50% increase of magnetic susceptibility in the upper 5 mm of the rhyolite sample. The basalt,
137 the microdiorite and the rhyolite are magnetically homogeneous at the sampling scale (~200
138 mg). The schist is heterogeneous at scale <1g: although the magnetic carriers have identical
139 hysteresis properties their concentration varies (and hence the magnetic susceptibility and
140 NRM) due to aggregation of pyrrhotite grains. The pre-shock magnetic properties are given in
141 Table 2. In summary, we studied four samples with the following dominant magnetic
142 mineralogy: multidomain magnetite (microdiorite), pseudo-monodomain Ti-rich
143 titanomagnetite (basalt), pseudomonodomain monoclinic pyrrhotite (schist) and monodomain
144 titanohematite (rhyolite). The direction of the NRM of each sample was measured on an
145 oriented fragment before the shock. The direction and intensity of the principal axis of
146 magnetic susceptibility (noted K1 and K3 for the maximum and minimum axes, respectively)
147 were evaluated on the same samples.

148

149 **6. Magnetic properties of shocked materials**

150 After measurement of the NRM (see next section), hysteresis parameters of shocked
151 samples were measured (Fig. 6). The plots of the hysteresis properties versus the distance to
152 the impact point show that for the basalt, the microdiorite and the schist, the coercivity and
153 the remanent magnetization at saturation increase close to the impact (Fig. 7). The effect,
154 already observed by Pesonen et al. (1997) is stronger for the microdiorite sample, with a five-
155 fold increase of both parameters. In all three cases, the intrinsic magnetic properties of all
156 samples are clearly modified by the shock wave. Various causes could explain the
157 modifications of magnetic properties: change in magnetic grain size, wall displacement in the
158 magnetic grains, shock-induced defects. We observed that the shock-induced changes in
159 hysteresis properties are not removed by stepwise heating up to 580°C. Therefore, these
160 modifications are not attributable to stress whose effects would be annealed at rather low
161 temperature (e.g. Van Velzen, 1992). Similarly, application of a strong field (up to 3 T) does
162 not reset the original magnetic properties. Therefore, wall displacements cannot be the cause
163 of the hysteresis modification. The only plausible explanation is a permanent modification of
164 the crystalline structure of the magnetite grains, namely microfractures, lattice defects or
165 dislocations.

166 The bulk magnetic susceptibility and the AMS (except for the rhyolite and the schist) were
167 measured after the shock. A slight decrease of magnetic susceptibility is observed for heavily
168 shocked (titano-)magnetite-bearing samples (Fig. 8), as already evidenced in previous works
169 (e.g. Hargraves and Perkins, 1969).

170 It is noteworthy that for the basalt (with a pre-shock minimum susceptibility axis K3 that is
171 about 30° away from the direction of impact), the heavily shocked samples have a higher
172 AMS degree (Fig. 9a) and their K3 axis is parallel to the direction of impact (Fig. 9b). For the
173 microdiorite (with a pre-shock K3 axis that is perpendicular to the direction of impact), away
174 from the impact point the K3 axes rotate from a direction parallel to the impact towards the
175 pre-impact direction (Fig. 9b). The intensity of the AMS for the microdiorite does not decay
176 away from the impact point as regularly as for the basalt, probably because we observe the
177 progressive superimposition of two different fabrics: the original one and the impact-induced
178 one. These observations show that the impact modified the existing magnetic fabric in the
179 first cm (peak pressure > 10 GPa) of the shocked basalt and microdiorite sample despite the
180 absence of visible macroscopic brecciation. The physical phenomena responsible for the
181 shock-induced magnetic anisotropy may be small-scale fracturing and deformation of
182 magnetite grains. It is unlikely that domain walls displacement by the shock wave is
183 responsible for even a small fraction of the shock-induced magnetic anisotropy. Indeed, the
184 magnetic anisotropy remains unchanged after application of high magnetic fields (3 T) that
185 would reset any domain wall displacement.

186

187 **7. Magnetization of shocked materials**

188 7.1. Demagnetization data

189 The NRM of all oriented sub-samples was measured and stepwise demagnetized with
190 alternating field (AF) up to 140 mT (Fig. 10). We also provide demagnetization data for
191 unshocked samples.

192 Unshocked basalt samples possess a single component of magnetization that is interpreted
193 as the original TRM. All shocked basalt samples possess a high coercivity component with a
194 direction close to the magnetization of the unshocked sample, that represents what is left from
195 the original TRM. The ~20° discrepancy between the pre- and post-shock high coercivity
196 directions is easily explained by summing the orientation uncertainties when drilling the pre-
197 and post-shock cores and when cutting and orienting the small parallelepipeds out of the post-
198 shock core. All shocked samples, even located at 3 cm from the impact (with an estimated
199 peak pressure of 2 GPa), have acquired a secondary component that is completely erased at 5
200 mT. This component of magnetization may be attributed to the shock or to the sawing
201 process. Basalt samples located close to the impact (< 1 cm, estimated peak pressure
202 > 10 GPa) possess a more stable secondary component isolated below 10 mT. This
203 component may be interpreted as a shock remanent magnetization (SRM) acquired in the

204 ambient magnetic field present during the explosion. However a thermoremanent origin
205 cannot be excluded for this low-coercivity component in view of the low blocking
206 temperatures of the basalt (see §4). Although poorly defined, the low coercivity directions are
207 not closely related to the ambient field at the time of impact (Fig. 11). They lie within the
208 plane defined by the pre-shock NRM and the ambient field.

209 For the microdiorite, the unshocked sample possesses two components of magnetization: a
210 low coercivity component, isolated below 6 mT, and a high coercivity component that is not
211 fully demagnetized at 150 mT. This latter component is interpreted as the original TRM.
212 Despite the low bulk coercivity of the microdiorite ($B_c = 2$ mT), its natural TRM is carried
213 by a high-coercivity fraction. The shocked samples still possess most of the original TRM.
214 The shocked samples located close to the impact (< 1.5 cm, peak pressure > 6 GPa) possess a
215 secondary component isolated below 30 mT and is interpreted as a SRM. The SRM directions
216 are scattered.

217 For the rhyolite, the unshocked sample possesses a single component of magnetization
218 carried by hematite. It is not clear if this original magnetization is a TRM or a chemical
219 remanent magnetization (see discussion in e.g. Vlag et al., 1997). All shocked samples
220 possess a high-coercivity component of similar direction than the original magnetization. The
221 shocked samples closest to the impact point (< 1 cm, peak pressure > 10 GPa) also possess a
222 low-coercivity component (SRM) isolated below ~ 30 mT. The SRM directions are scattered.

223 The pyrrhotite-bearing schist did not provide stable directions of NRM when demagnetized
224 by alternating field (Fig. 10). Therefore we will not discuss the possible remagnetization in
225 the shocked schist.

226

227 7.2. Remagnetization and demagnetization by shock

228 In our experiments, since the directions of the original TRM and the SRM are different we
229 cannot simply compare the intensities of the pre- and post-shock NRM. For the basalt for
230 instance, the intensity of the total post-shock NRM is much lower than the sum of the
231 intensities of the two components of magnetization (e.g. sample B5 of Fig. 10). In figure 12,
232 we plot the scalar sum of the intensities of the stepwise-demagnetized magnetization vectors
233 for basalt and microdiorite samples. The intensities are normalized to the saturation
234 magnetization of each sample to take into account the natural variability in ferromagnetic
235 mineral concentration. After the shock, the sum of the intensities of the different components
236 of magnetization is weaker than before the shock for the basalt, but higher for the
237 microdiorite. The basalt is globally demagnetized whereas the microdiorite is globally

238 remagnetized by the shock. To our knowledge, this is the first time that shock experiments
239 actually increase the original NRM of a rock. The increase of the magnetization of the
240 microdiorite after the shock does not mean that SRM acquisition is more efficient than TRM
241 acquisition. This is due to the increased capacity of the microdiorite to acquire a remanent
242 magnetization after the shock (i.e. increase of M_r/M_s by a factor up to five) and primarily to
243 the fact that the original remanence was carried almost entirely by the grains with high
244 coercivity so that the shock added a secondary low-coercivity SRM to the original high-
245 coercivity TRM that was not much affected by the shock.

246 In view of the rather unstable behaviour of the NRM of the microdiorite and the schist
247 under AF demagnetization and the high resistance of the NRM of the rhyolite to AF
248 demagnetization (Fig. 10), only the basalt was suitable for a detailed study of the effect of
249 shock on the remanence. For the basalt that has a simple demagnetization behaviour under
250 alternating field and a TRM carried by grains spanning the whole coercivity spectrum, we can
251 compare the magnetization slope ($dNRM/dAF$) for shocked and unshocked samples as a
252 function of the peak alternating field (Fig. 13). Above 10-15 mT, all shocked samples located
253 more than 15 mm from the impact point (peak pressure < 6 GPa) closely follow the curve for
254 the unshocked basalt. Contrarily, heavily shocked samples (B5 to B14) plot below the
255 unshocked samples between 10 and 40 mT. Above 40 mT all curves are identical. On the
256 interval 10-40 mT, these heavily shocked samples have a magnetization that has the same
257 direction as the original TRM. This means that the original TRM of samples B5 to B14 has
258 been partly demagnetized on the 10-40 mT coercivity window. If a SRM or a TRM has been
259 acquired on the same coercivity window during the shock, it is small enough not to be
260 noticeable on the demagnetization plot, i.e. it is at most a few % of the original TRM. We can
261 quantify the shock demagnetization of the original TRM on the 10-40 mT coercivity interval
262 by comparing the amount of NRM demagnetized between 10 mT and 40 mT for pre- and
263 post-shock samples (fig. 14). Up to a distance of 14 mm from the impact, corresponding to a
264 peak pressure of about 7 GPa (sample B14), the original TRM of shocked samples has been
265 significantly demagnetized. For sample B5 that has suffered peak pressure around 20 GPa, the
266 original TRM has been divided by up to a factor 5. It is noteworthy that attempting a
267 paleointensity measurement on such a shocked sample would be problematic since it is
268 impossible to notice that part of the TRM has been demagnetized by shock. Although it is not
269 clear how this demagnetization is dispatched along the blocking temperature spectrum, the
270 paleointensity experiment would at best provide an underestimated value (up to a factor 5 in
271 the case of sample B5 for instance).

272 Generally speaking the effect of the explosive-driven shocks on the NRM of the four
273 studied lithologies appear rather weak compared to a number of previous studies performed
274 on isothermal remanent magnetization (IRM). Complete demagnetization of the IRM of a
275 titano-magnetite bearing basalt shocked with a laser pulse was observed at about 2 GPa
276 (Gattacceca et al. 2006). Shock experiments with a gas gun on pyrrhotite-bearing samples
277 showed a 80% demagnetization of IRM at only 0.5 GPa (Louzada et al., in press). The large
278 differences are attributed to the fact that NRM and IRM react differently to shock waves.

279

280 **8. Conclusion**

281 Experimental shocks of four rocks with different lithology and magnetic mineralogy show
282 that, in most cases (only the hematite case is not conclusive), the intrinsic magnetic properties
283 of the rock are permanently modified by the shock wave. A remarkable effect, not
284 documented in previous studies, is the capacity of the shock wave to superimpose a new
285 fabric (with a minimum susceptibility axis parallel to the direction of impact) to the original
286 magnetic fabric of the rock. Multidomain magnetite-, pseudo-single domain titanomagnetite-
287 and monoclinic pyrrhotite-bearing rocks show a noticeable increase of their coercivity for
288 pressure above 10 GPa. These changes are not annealed even at high temperature (580 °C).
289 They are attributed to fracturing and/or dislocations of the ferromagnetic grains. This
290 fracturing is also responsible for the appearance of a shock-induced anisotropy of magnetic
291 susceptibility. These results show that the magnetic properties of meteorites which are
292 commonly shocked to pressures well above 10 GPa (e.g. Martian meteorites, Nyquist et al.,
293 2001) may not be representative of the magnetic properties of their parent body.

294 For (titano)magnetite bearing rocks, we observe both a shock demagnetization of the original
295 TRM for magnetic grains with coercivity up to 40 mT, and a possible shock magnetization for
296 grains with coercivity up to 10 mT. NRM appears to be much more resistant to shock than
297 IRM (probably because they have different coercivity spectra), implying that more work is
298 needed on the effects of shock on natural magnetization. As observed by Cisowski and Fuller
299 (1978), the demagnetizing effects of the shock wave depend closely on the coercivity
300 spectrum of the grains carrying the original remanence, and the shock-remagnetizing effect
301 depend on the presence (or creation by the impact itself) of low-coercivity magnetic grains.
302 With an impact occurring in an ambient magnetic field of similar intensity to the original
303 magnetizing field, the post-shock magnetization may be higher or lower than the pre-shock
304 magnetization depending on these two factors.

305 To summarize, although an impact occurring after dynamo shutdown will indeed demagnetize
306 the crust to a variable extent, an impact occurring while the dynamo is still active may
307 demagnetize the crust almost as efficiently or conversely may lead to the situation where the
308 shocked crust has a stronger magnetization than the surrounding rocks (depending on the
309 efficiency of SRM acquisition, and on the nature of the original NRM). Therefore, it appears
310 difficult to draw conclusions about the dynamo history of a planet by studying the magnetic
311 anomalies above its impact basins, unless the anomalies provide information about the
312 magnetization of the rocks heated during the impacts (if they are preserved). The decisive clue
313 to the presence of an active dynamo at the time of impact is the presence or absence of a
314 thermoremanence carried by the volume of rocks heated above blocking temperatures during
315 the impact. Similarly, it may be difficult to determine which magnetic phase dominates the
316 crust based only on the demagnetization pattern around impact basins.

Accepted Manuscript

Acknowledgements

This work was supported by the Programme National de Planétologie (INSU/CNES, France). We acknowledge very constructive comments by S. T. Stewart-Mukhopadhyay and an anonymous reviewer.

References

- Auroux, E., and Deleignies, M., 2003. Sensitivity of the EOS of detonation products to the parametrization of the intermolecular potential for pure fluids in thermomechanical calculations. Proceedings of 5th international Symposium of high dynamic pressures, CEA eds, p. 281.
- Cogné, J.P., 2003. PaleoMac: a Macintosh™ application for treating paleomagnetic data and making plate reconstructions. *Geochem. Geophys. Geosyst.*, 4, doi:10.1029/2001GC000227.
- Cisowski, S.M., and Fuller, M., 1978. The effect of shock on the magnetism of terrestrial rocks. *J. Geophys. Res.*, 83: 3441-3456.
- Dickinson, T.L., and Wasilewski, P., 2000. Shock magnetism in fine particle iron. *Meteor. Planet. Sci.*, 35: 65-74.
- Dunlop, D.J., and Özdemir, Ö., 1997. *Rock magnetism: fundamentals and frontiers*. Cambridge University Press, Cambridge, 573 pp.
- Gattacceca, J., Boustie, M., Weiss, B.P., Rochette, P., Lima, E., Fong, L.E., and Baudenbacher, F., 2006. Investigating impact demagnetization through laser impacts and SQUID microscopy. *Geology*, 34: 333-336.
- Hargraves, R.B., and Perkins, W.E., 1969. Investigations of the effect of shock on natural remanent magnetism. *J. Geophys. Res.* 74: 2576-2589.
- Halekas, J.S., Lin, R.P., and Mitchell, D.L., 2003. Magnetic fields of lunar multi-ring impact basins. *Meteor. Planet. Sci.*, 38: 565-578.
- Hood, L., Richmond, N.C., Pierazzo, E., and Rochette, P., 2003. Distribution of crustal magnetic fields on Mars: shock effects of basin-forming impacts. *Geophys. Res. Lett.*, 30, doi: 10.1029/2002GL016657.
- Kletetschka, G., Eonnerney, J.E.P., Ness, N.F., and Acuña, M.H., 2004. Pressure effects on martian crustal magnetization near large impact basins. *Meteor. Planet. Sci.*, 39: 1839-1848.

- Louzada, K., Stewart, S.T., and Weiss, B.P., 2005. The effect of shock on the magnetic properties of pyrrhotite, the Martian crust, and meteorites. *Geophys. Res. Lett.*, in press.
- Martelli, G., and Newton, G., 1977. Hypervelocity cratering and impact magnetisation of basalt. *Nature*, 269: 478-480.
- Nyquist, L.E., Bogard, D.D., Shih, C.Y., Greshake, A., Stöffler, D., Eugster, O., 2001. Ages and geologic histories of Martian meteorites. *Space Sci. Reviews*, 96: 105-164.
- Pesonen, L.J., Deutsch, A., Hornemann, U., and Langenhorst, F., 1997. Magnetic properties of diabase samples shocked experimentally in the 4.5 to 35 GPa range. 28th Lunar and Planetary Science Meeting: 1087-1088.
- Pilkington, M., and Grieve, R.A.F., 1992. The geophysical signature of terrestrial impact craters. *Rev. Geophysics*, 30: 161-181.
- Pohl, J., Bleil, U., and Hornemann, U., 1975. Shock magnetization and demagnetization of basalt by transient stress up to 10 kbar. *J. Geophysics*, 41: 23-41.
- Rochette, P., Bertrand, H., Braun, C., and Berger, E., 1993. La province volcanique Pléistocène supérieur du Bas-Vivarais (Ardèche, France) : propagation de fentes crustales en échelons ? *C. R. Acad. Sci. Paris*, 316: 913-920.
- Srnka, L.J., Martelli, G., Newton, G., Cisowski, S.M., Fuller, M.D., and Schaal, R.B., 1979. Magnetic field and shock effects and remanent magnetization in a hypervelocity impact experiment. *Earth Planet. Sc. Lett.*, 42: 127-137.
- Stöffler, D., Keil, K., and Scott, E.R.D., 1991. Shock metamorphism of ordinary chondrites. *Geochim. Cosmochim. Acta*, 55: 3845-3867.
- Van Velzen, A.J., and Zijderfeld, J.D.A., 1992. A method to study alterations of magnetic minerals during thermal demagnetization applied to a fine-grained marine marl (Trubi formation, Sicily). *Geophys. J. Int.*, 110: 79-90.
- Vlag, P., Vandamme, D., Rochette, P., and Spinelli, K., 1997. Paleomagnetism in the Esterel rocks: a revisit 22 years after the thesis of H. Zijderfeld. *Geologie en Mijnbouw*, 76: 21-33.
- Wilkins, M.L., 1999. Computer simulation of dynamic phenomena. Springer eds, New York, 246 pp.

Figure captions

- Figure 1 - Sketch illustrating the different steps of the sampling after explosion. The wire used to saw the parallelepipeds is 220 μm in diameter.
- Figure 2 - Modelled pressure versus time at various depths in the rock straight below the explosion. The modelling was performed with a Johnson Wilkins Lee law for the explosive and the Radioss code for the shock wave propagation in the sample (see text).
- Figure 3 - Peak pressure versus depth in the rock straight below the explosion. The pressure values are deduced from the shock wave modelling presented in Fig. 2. The solid line is computed with a density of 2300 kg.m^{-3} , the dashed line is computed with a density of 3000 kg.m^{-3} .
- Figure 4 - Modelled peak temperature versus depth in the sample straight below the explosion, considering the amount of heat transferred to the to by the explosion of the PETN detonator. Dashed line is at 50°C. The modelling was performed using Carte and FEMLAB codes (see text).
- Figure 5 - Thermomagnetic curves for the four studied lithologies (susceptibility vs. temperature). Empty circles indicate the beginning of the heating curves. Heating = thick lines, cooling = thin lines. For the basalt and the microdiorite, progressive TRM acquisition curves are also plotted (dotted line, with standard deviation when available).
- Figure 6 - Representative hysteresis loops for shocked and unshocked samples of the four studied lithologies. The loops have been corrected for the paramagnetic slope.
- Figure 7 - Hysteresis properties vs. depth for the shocked samples (M_r : remanent magnetization at saturation, M_s : saturation magnetization, B_{cr} : coercivity of remanence, B_c : coercivity). Dashed line is the mean value for unshocked samples (grey band = one standard deviation).
- Figure 8 - Low-field specific magnetic susceptibility of impacted samples. Pre-impact mean are indicated with one standard deviation (grey bands).
- Figure 9 - a-c) Degree of anisotropy of magnetic susceptibility (P_{ams} = ratio of maximum to minimum principal susceptibility values) vs. distance to the impact. Pre-impact means are indicated (dashed line) with one standard deviation (grey bands). b-d) Lower-hemisphere equal area stereographic projection of minimum axis of magnetic susceptibility K_3 .
- Figure 10 - Orthogonal demagnetization plots of oriented samples of the shocked rocks. Open and solid symbols represent projections of the magnetization vector on vertical and horizontal planes, respectively. Demagnetization plots for oriented unshocked samples are given for comparison. Demagnetization steps are 5, 10, 15, ..., 50, 60, 70, 80, 100, 120, 140 mT.
- Figure 11 - Equal-area stereographic projection of the directions of magnetization (0° = North and 90° = East in Fig. 10). Open (solid) dots represent projection onto upper (lower) hemisphere. Open ellipses are the projections of the 95% confidence cones about the directions. Diamond: ambient field during the impact; K_1 (resp. K_3) : maximum (resp. minimum) susceptibility principal axis, large labelled circles: low-coercivity components, small circles: high-coercivity components; large labelled star: pre-impact direction of magnetization (determined on a separate core), star: mean direction of the high-coercivity components of shocked samples.
- Figure 12 - Sum of demagnetized vectors (scalar intensity) normalized by saturation magnetization vs. distance from the impact. The dotted line represents an unshocked sample.
- Figure 13 - NRM slope ($d\text{NRM}/d\text{AF}$) as a function of alternating field for shocked basalt samples. The curve for pre-shock NRM (dashed line) is plotted for comparison. Curves are normalized to saturation magnetization (M_s) to take into account the possible variability in titanomagnetite content. Data for demagnetizing field below 10 mT are not represented

because the origin of the low coercivity component is not ascertained for the basalt (see text).

Figure 14 - Mean degree of shock demagnetization of the basalt on the 10-40 mT coercivity window as a function of distance to impact. This value is derived from the ratio of the NRM moment demagnetized between 10 mT and 40 mT before and after shock.

Accepted Manuscript

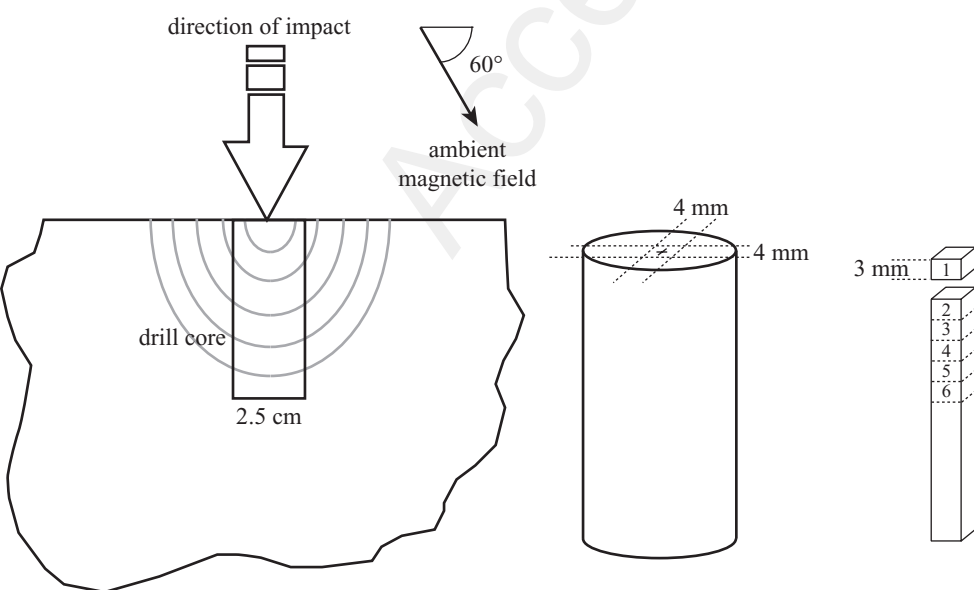


Figure 1

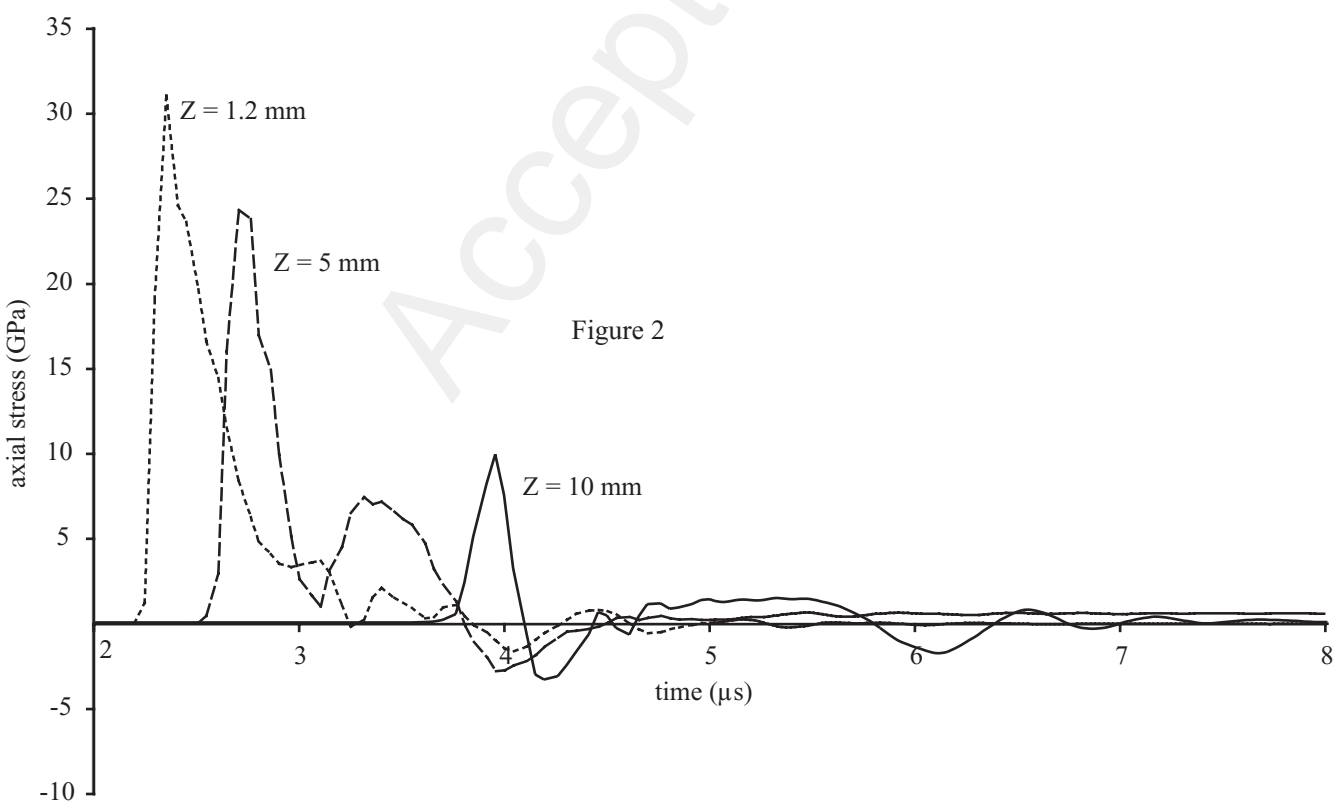
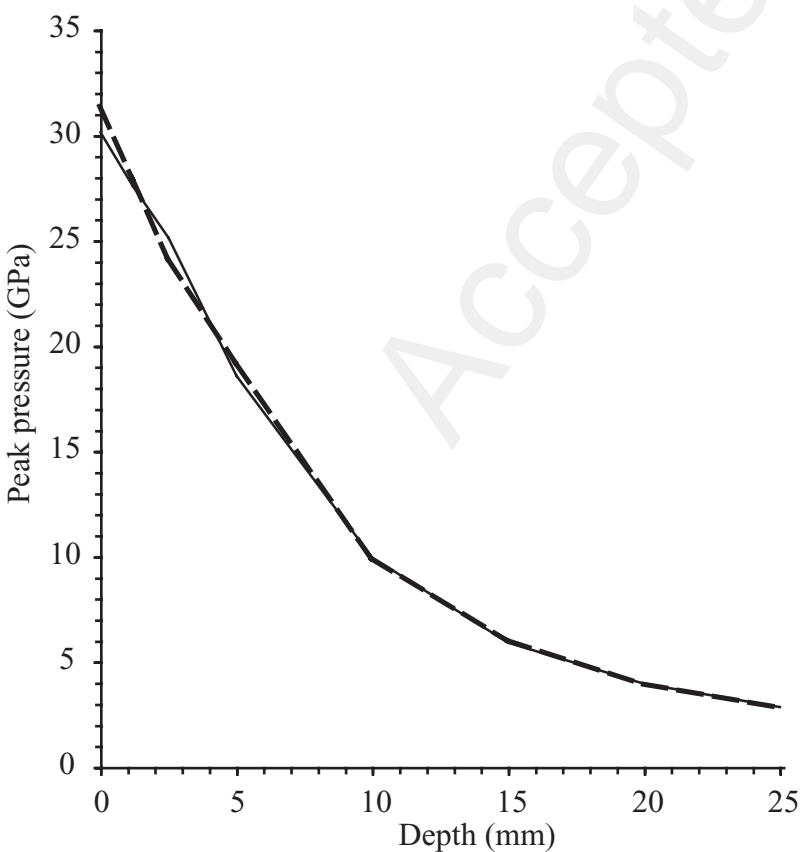


Figure 2



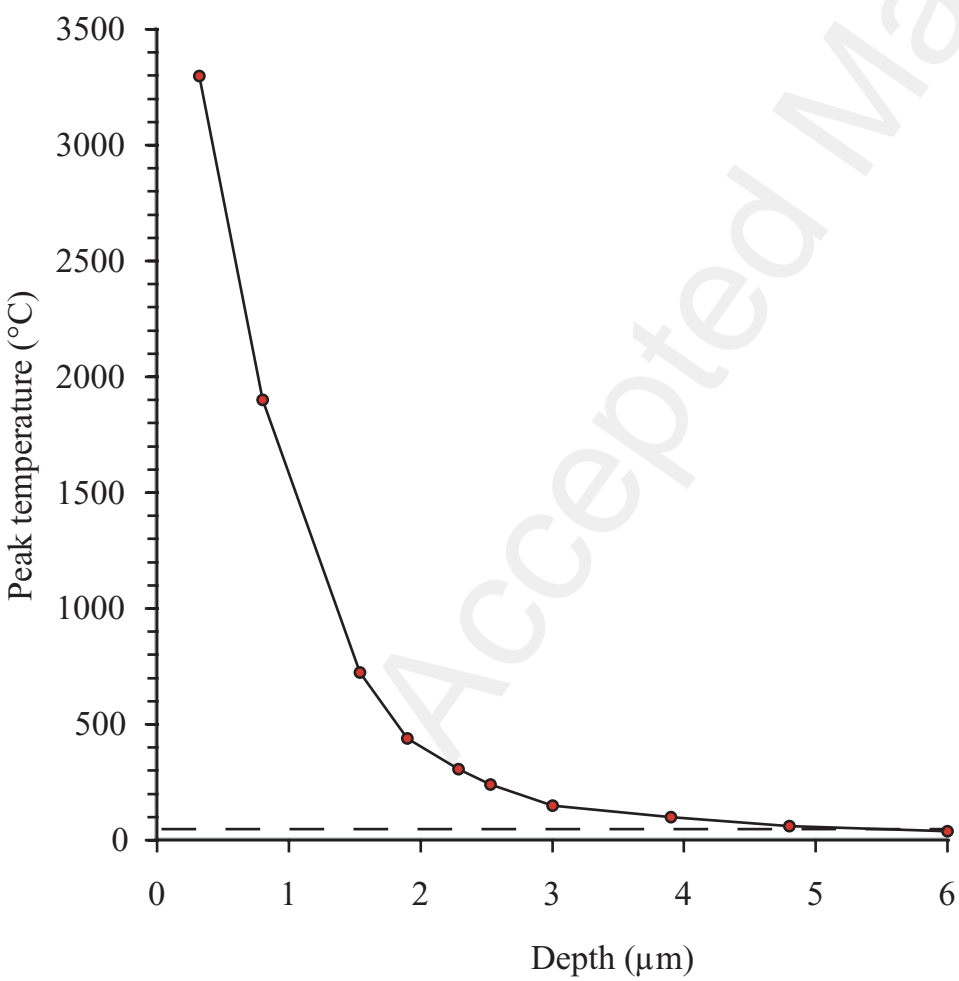
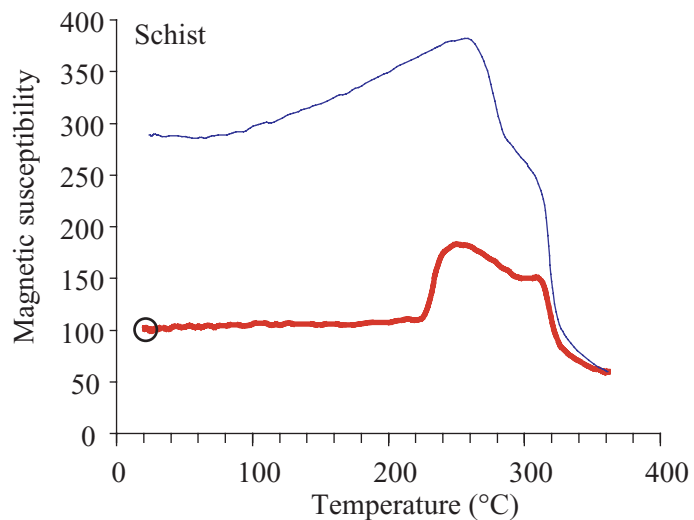
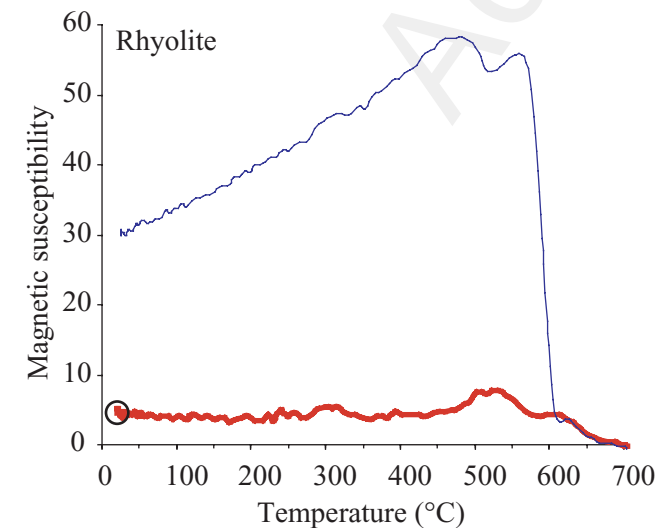
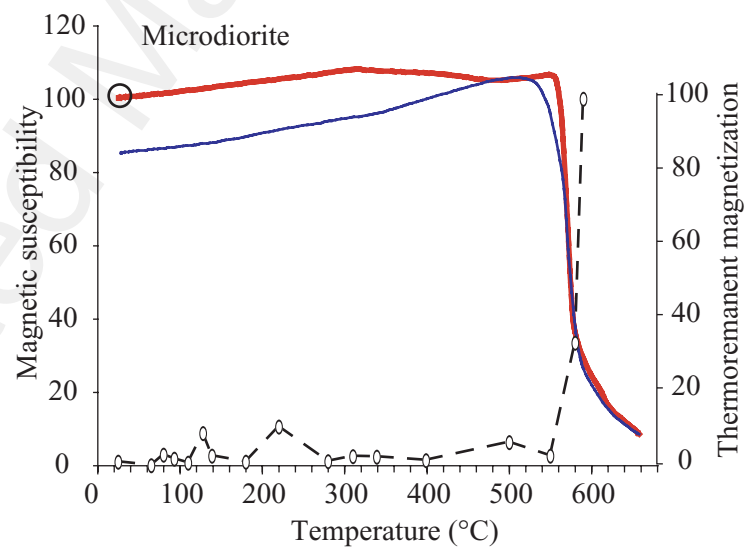
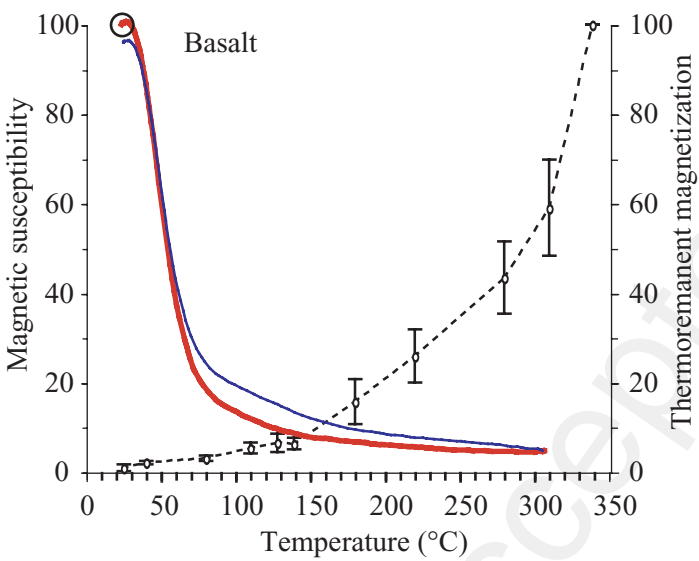
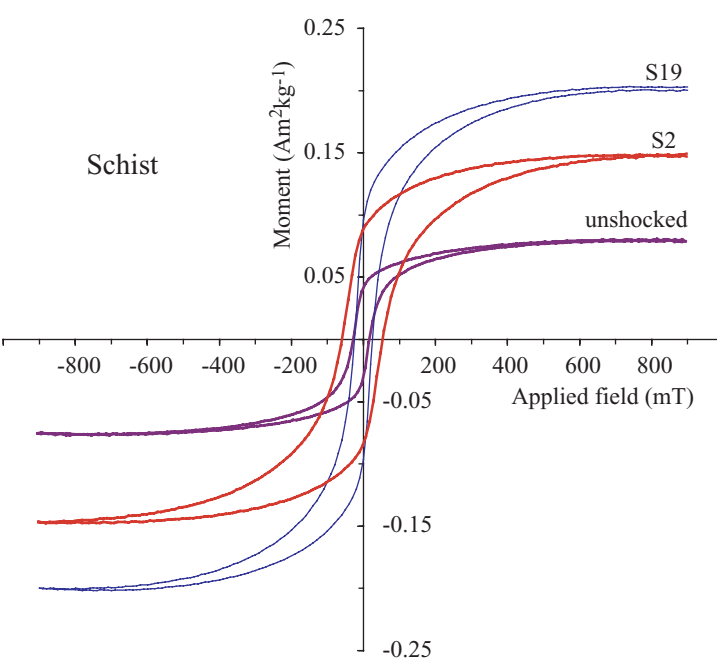
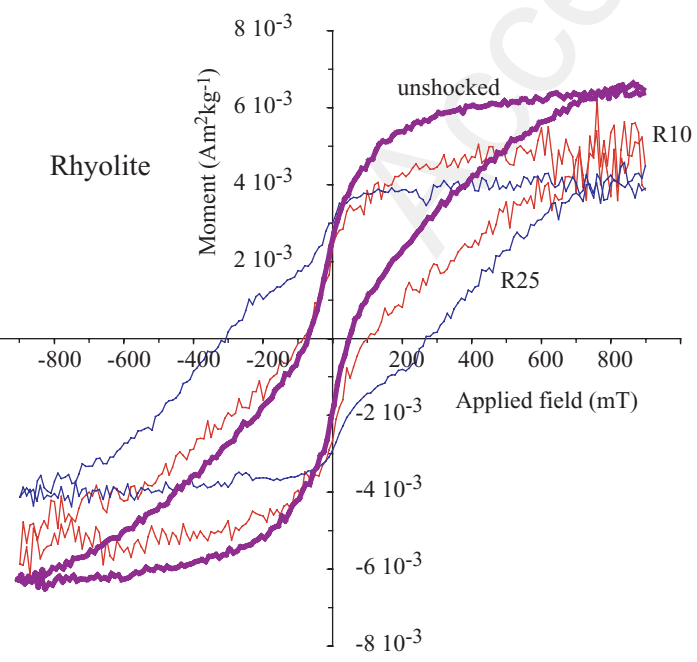
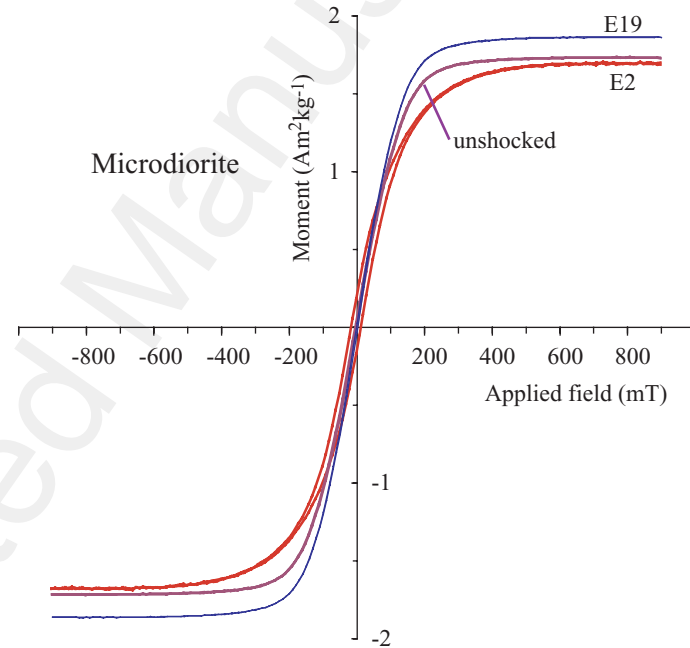
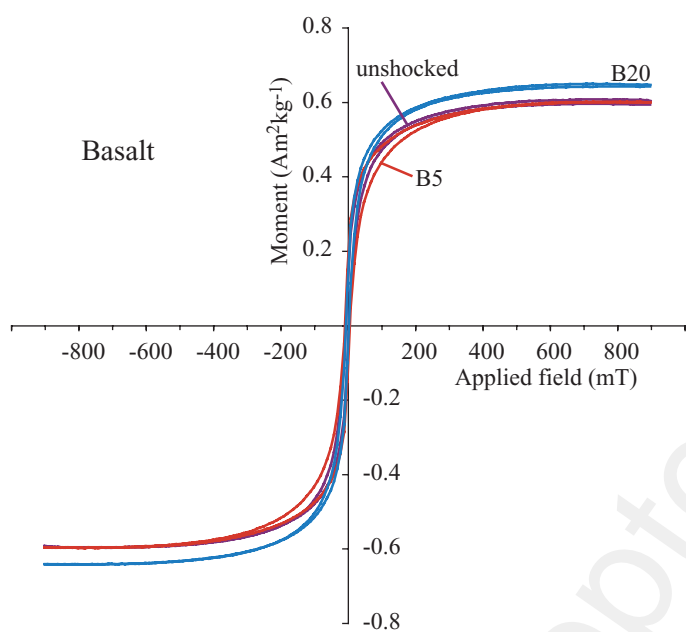
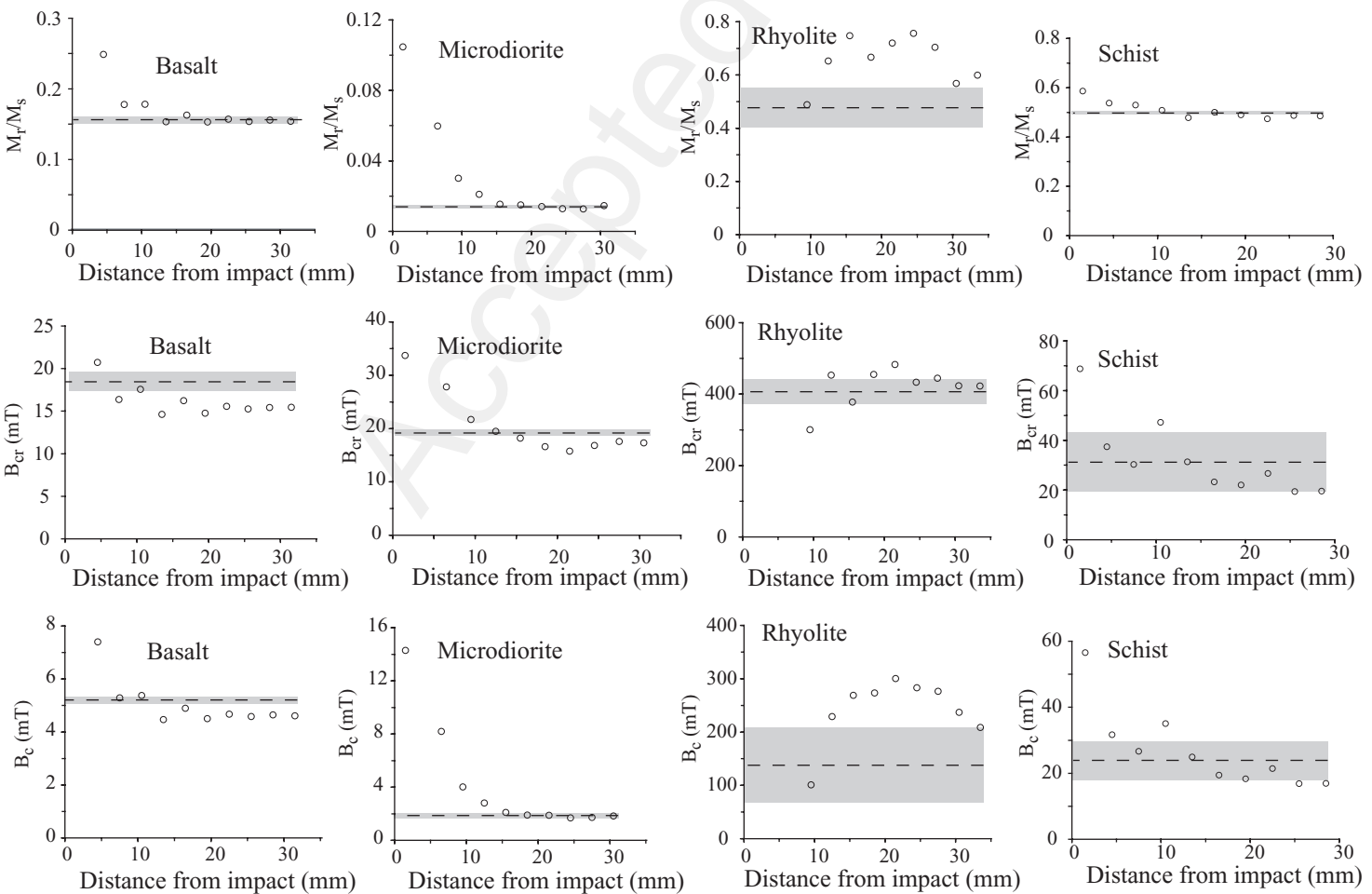
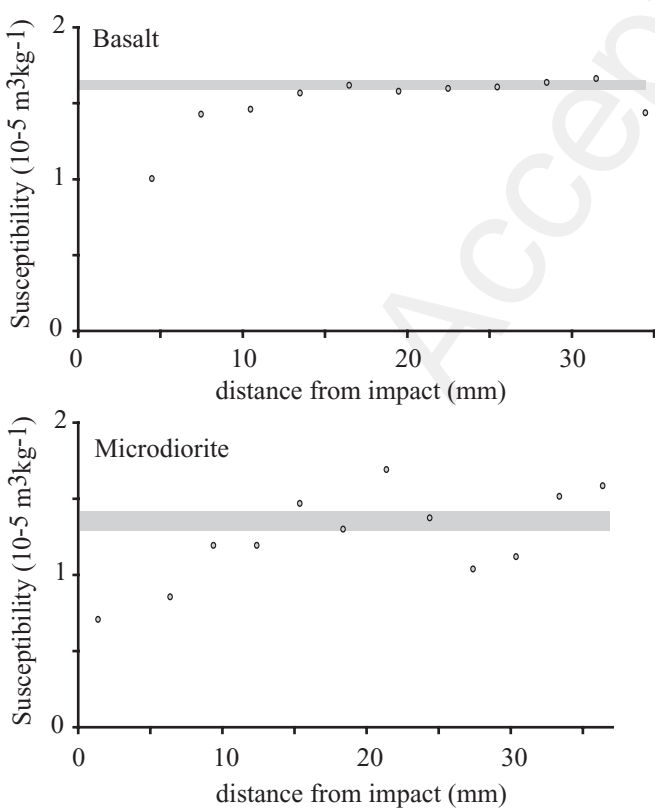


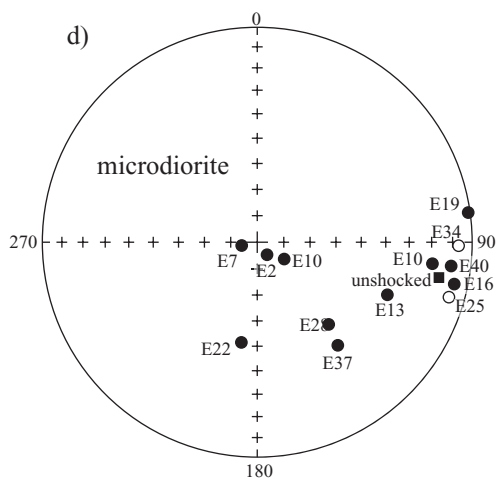
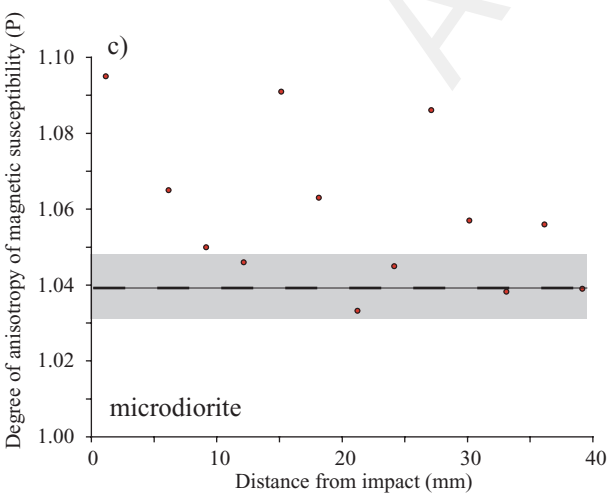
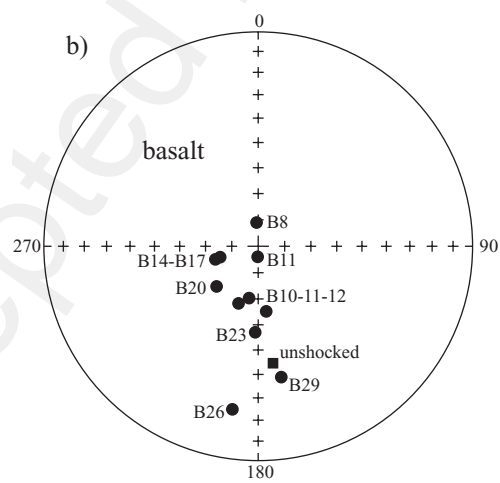
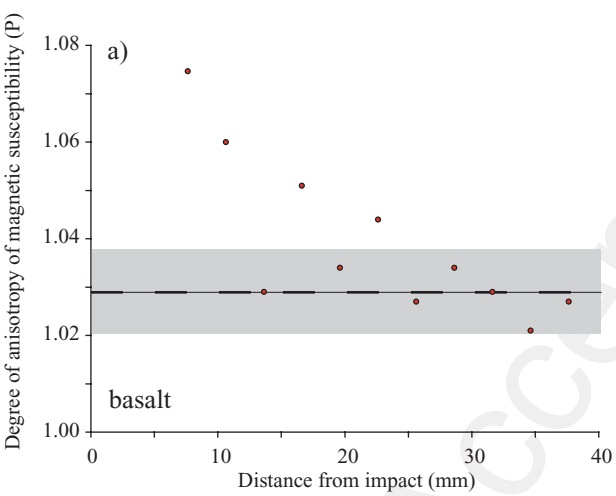
Figure 4

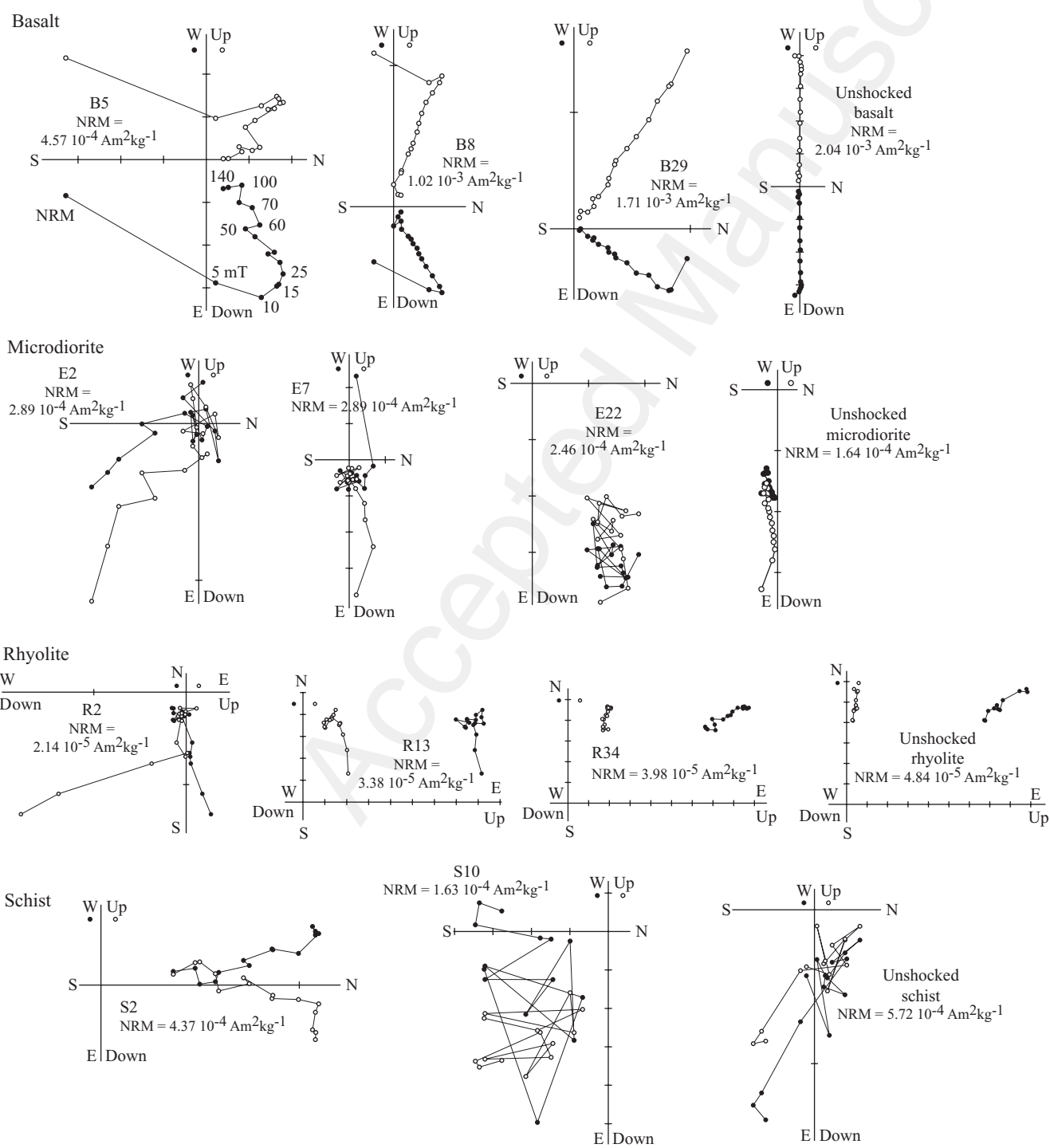


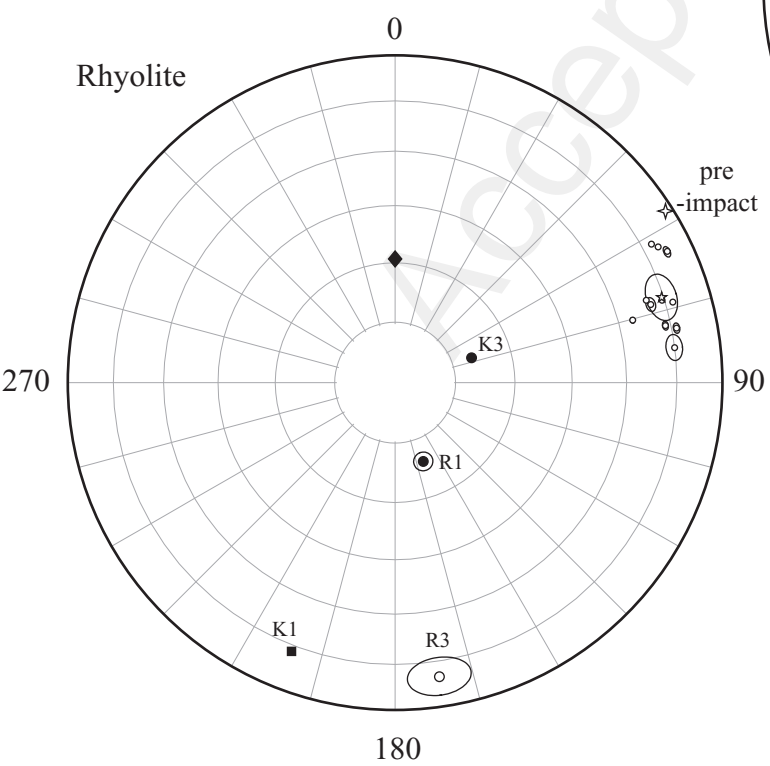
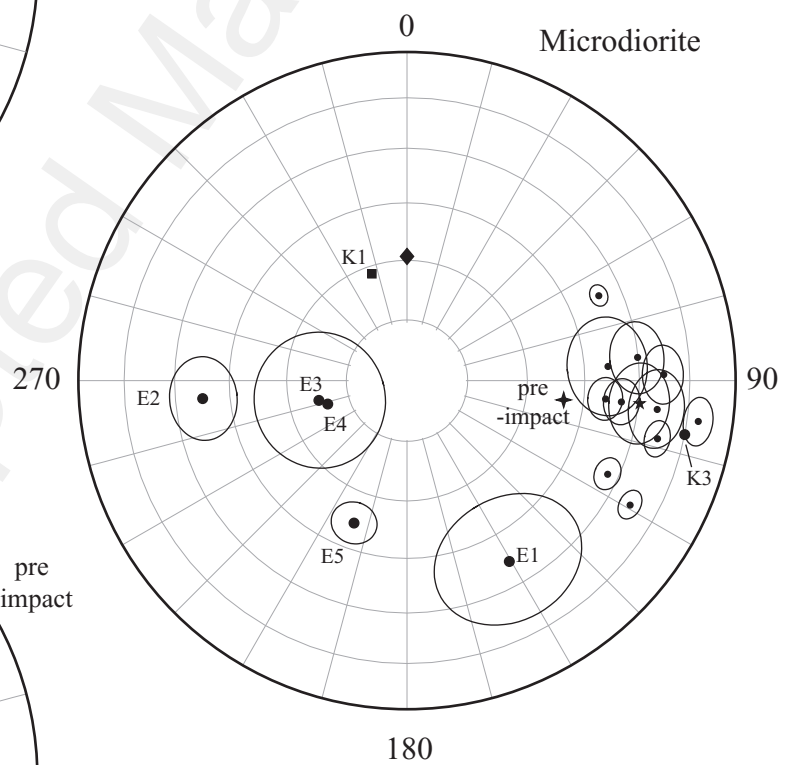
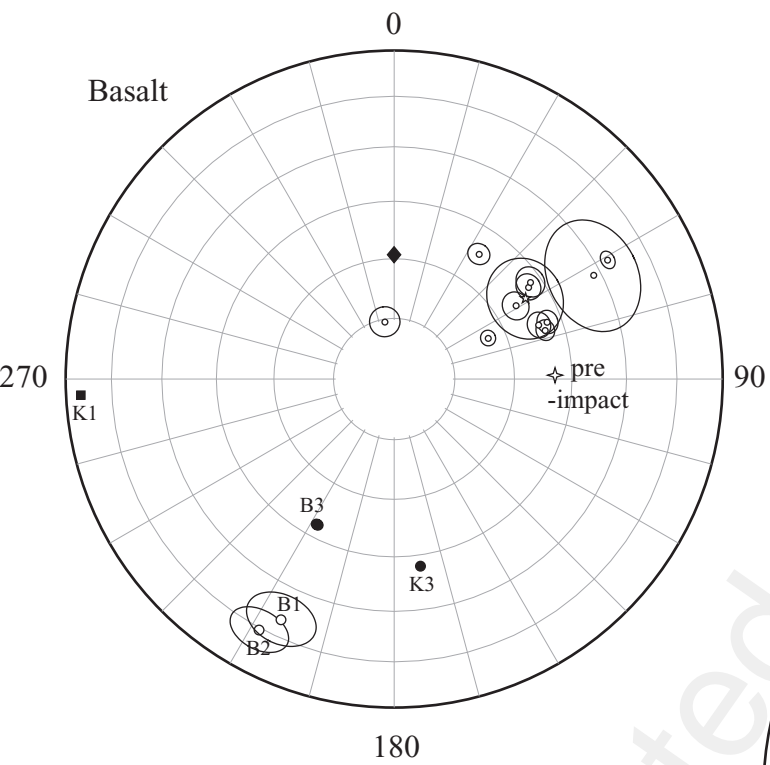


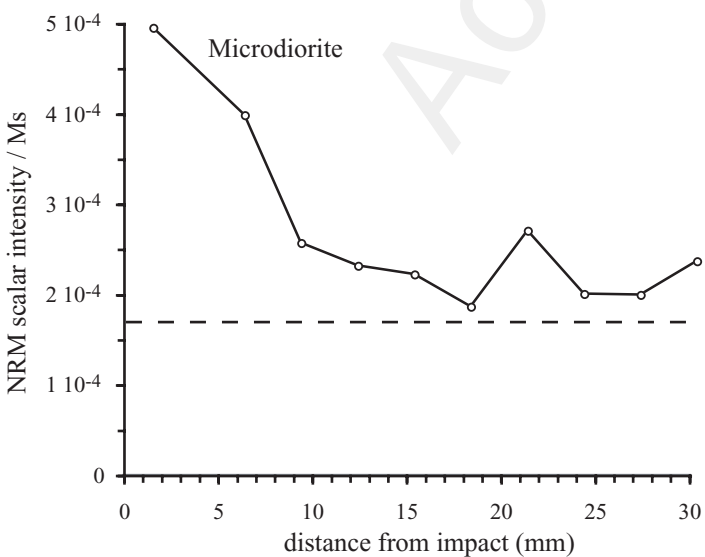
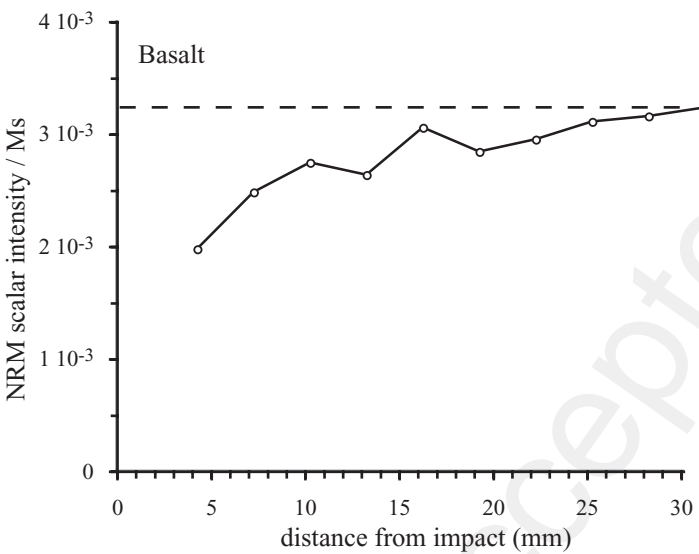


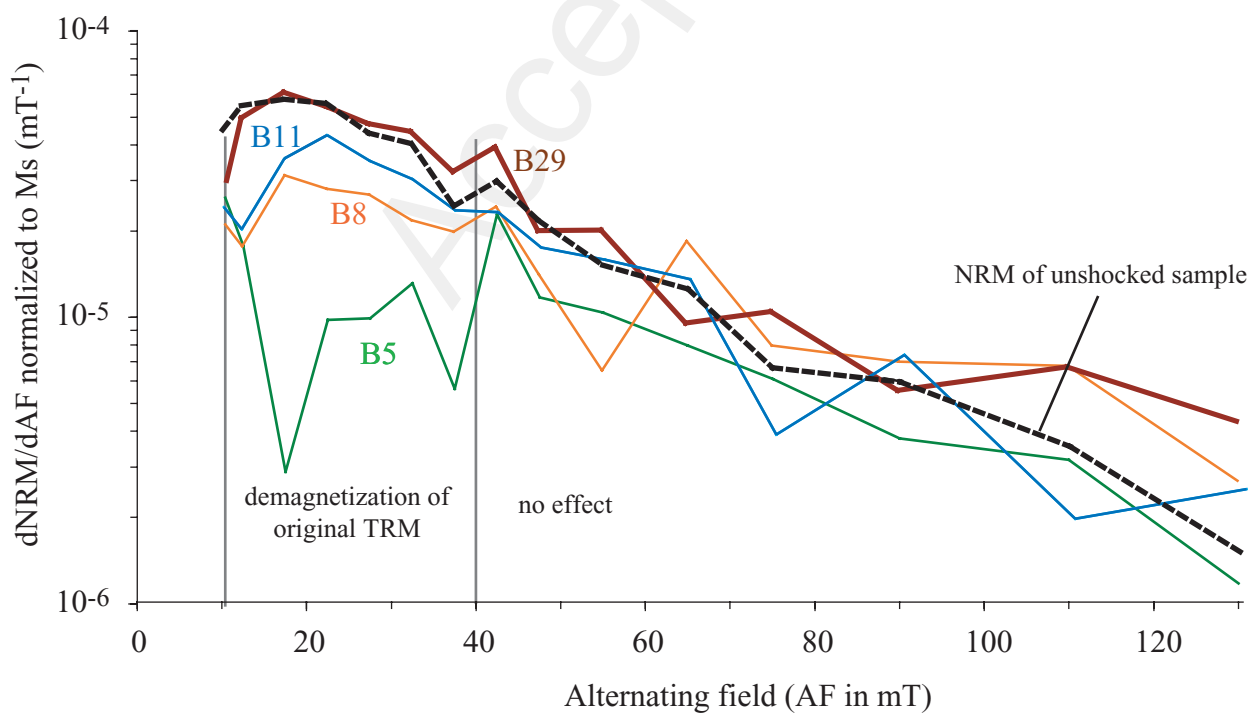


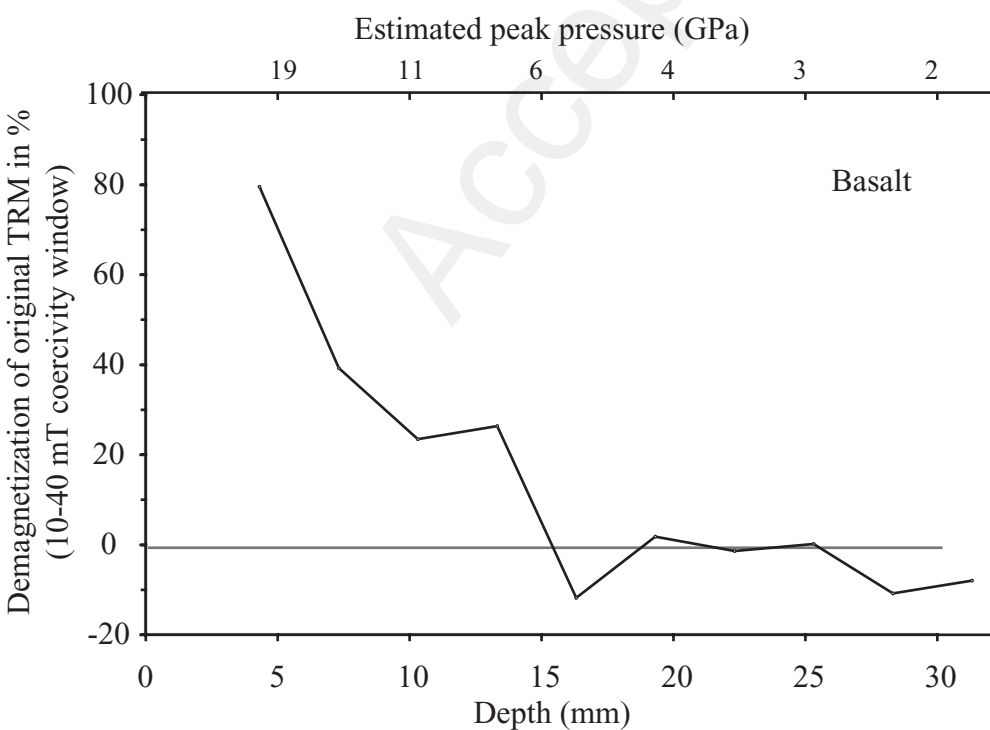












Tables

Table 1 - Physical parameters used in the shock and thermal simulations.

Explosive (PETN)	ρ_0 (g.cm ⁻³)	D (m.s ⁻¹)	P _{CJ} (GPa)	A (GPa)	B (GPa)	R ₁	R ₂	ω
	1.77	8300	33.35	617	16.93	4.4	1.2	0.25
Basalt	ρ_0 (g.cm ⁻³)	C ₀ (m.s ⁻¹)	S	Γ	Y ₀ (GPa)	k (W.m ⁻¹ .K ⁻¹)	C (J.kg.K ⁻¹)	
	2.88	4800	1.34	2	0.3	1.99	1000	

ρ_0 : density; D: shock speed; P_{CJ}: Chapman-Jouguet pressure; A, B, R₁, R₂: JWL parameters associated to the JWL equation mentioned in the text (Wilkins, 1999); ω : Grüneisen coefficient; C₀: sound speed; S: empirical parameter; Γ : Grüneisen coefficient; Y₀: yield stress; k: thermal conductivity; C: heat capacity.

Table 2 - Magnetic properties of materials before shock

	Basalt	Microdiorite	Rhyolite	Schist
Hysteresis	n=10	n=12	n=10	n=10
Mr (Am ² kg ⁻¹)	9.78 ± 0.67 10 ⁻²	2.38 ± 0.20 10 ⁻²	2.31 ± 0.22 10 ⁻³	4.48 ± 2.90 10 ⁻²
Ms (Am ² kg ⁻¹)	6.22 ± 0.46 10 ⁻¹	1.28 ± 0.14 10 ⁻¹	4.91 ± 0.72 10 ⁻³	9.14 ± 6.02 10 ⁻²
Mr/Ms	1.57 ± 0.03 10 ⁻¹	1.39 ± 0.07 10 ⁻²	4.77 ± 0.73 10 ⁻¹	4.99 ± 0.28 10 ⁻¹
Bc (mT)	5.19 ± 0.16	1.86 ± 0.08	137 ± 69	23.8 ± 5.9
Bcr (mT)	18.4 ± 1.1	19.1 ± 0.7	406 ± 35	31.3 ± 11.7
Bcr/Bc	3.54 ± 0.14	10.3 ± 0.4	3.56 ± 1.47	1.29 ± 0.12
Susceptibility	n=22	n=28	n=9	n=7*
Susceptibility (m ³ kg ⁻¹)	1.61 ± 0.03 10 ⁻⁵	1.35 ± 0.07 10 ⁻⁵	3.31 ± 0.58 10 ⁻⁸	3.19 ± 0.20 10 ⁻⁷
AMS	n=8	n=8		
Anisotropy degree	1.029 ± 0.009	1.040 ± 0.008		
Magnetization	n=14	n=13	n=19	n=7*
NRM (Am ² kg ⁻¹)	1.70 ± 0.22 10 ⁻³	1.71 ± 0.12 10 ⁻⁴	4.19 ± 0.44 10 ⁻⁵	6.60 ± 2.84 10 ⁻⁵

For each magnetic property, the number of measured samples (n) is indicated.

* For susceptibility and magnetization of the schist, only samples with mass > 1g have been taken into account due to small-scale heterogeneities in pyrrhotite concentration.